Chinese Chemical Letters 31 (2020) 2871–2875

Contents lists available at ScienceDirect

Chinese Chemical Letters

journal homepage: www.elsevier.com/locate/cclet

Communication

Efficient silver nanocluster photocatalyst for simultaneous methyl orange/4-chlorophenol oxidation and Cr(VI) reduction

Liming Peng[a,b], Yucui Bian[a], Xiaoqing Shen[b,*], Hong-Chang Yao[a], Haijun Chen[a,*], Zhongjun Li[a]

[a] College of Chemistry, and Institute of Green Catalysis, Zhengzhou University, Zhengzhou 450001, China
[b] College of Materials Science and Engineering, Zhengzhou University, Zhengzhou 450001, China

ARTICLE INFO

Article history:
Received 4 April 2020
Received in revised form 21 April 2020
Accepted 1 June 2020
Available online 2 June 2020

Keywords:
Metal cluster
Silver nanocluster
Photocatalysis
Synchronous degradation
Water pollutants
$O_2^{\bullet-}$ radical

ABSTRACT

Metal nanoclusters have shown great potential in photocatalysis, while simultaneous removal of both inorganic and organic contaminants by metal nanoclusters under visible light is less explored. Here, we synthesized $Ag_m(SR)_n$ (SR represents 3-mercaptopropyltriethoxysilane ligand) nanoclusters (~1 nm) *via* a reduction of silver triphenylphosphine under ambient conditions in the presence of 3-mercaptopropyltriethoxysilane. The nanocluster was characterized by UV–vis spectroscopy, high resolution transmission electron microscopy (HRTEM), Fourier transform infrared spectrum (FTIR), and X-ray photoelectron spectroscopy (XPS). Under 5 W blue LED, the $Ag_m(SR)_n$/P25 exhibits enhanced catalytic activity for simultaneous methyl orange (MO) oxidation and Cr(VI) reduction, and also for synchronous 4-chlorophenol oxidation and Cr(VI) reduction. Mechanism studies by electrochemical impedance spectroscopy (EIS), photoluminescence (PL), electron spin resonance (ESR) *etc.* and control experiments reveal that the unique structure of silver nanoclusters with thiolate ligands is vital to the high catalytic performance, and both the photo-generated holes and superoxide radicals are responsible for the decomposition of MO.

Metal nanoclusters (NC, < 2 nm), usually consisting of a few to a hundred atoms, and the sizes of which are comparable to the Fermi wavelength of electrons, have attracted special attention in catalysis, bioimaging, and many other areas due to their unique physicochemical properties [1–6]. Such materials exhibit molecular-like properties originating from quantum confinement effects, which manifest HOMO-LUMO gap. The energy gap of nanoclusters generally falling into visible light energy region makes them appropriate candidates for visible light photocatalysis.

Due to intentional industrial dumping and agricultural activity, water pollution, including both inorganic metal ions (such as Cr(VI)) and organic compounds (such as phenols), has become one of the primary environmental problems that human being is facing and straightly harms the Earth's health of life [7,8]. To eliminate these contaminants, visible light-driven photocatalysis, which is one of the most promising and eco-friendly method [9,10], has drawn increasing attention for water purification and environmental protection because of low energy consumption [11,12]. In order to maximize the solar energy conversion efficacy, efficient and stable nanomaterials are needed to collect visible light [13]. Apart from semiconductor photocatalysts, well-dispersed noble metal nanoparticles with unique surface plasmon resonance (LSPR) were explored as visible light response assistant in photocatalysis [14–17]. Recently, it was found that hot carriers generated from interband transitions are more efficient than those carriers generated merely by LSPR in catalysis [18], especially thiolate protected nanoclusters with discrete energy structure have attracted mustard interest and used as photosensitizers in light harvesting and conversion process [19–21], which may provide an alternative route to the development of photocatalysts.

As for the photocatalytic degradation, inorganic and organic pollutions usually coexist in waste water, thus harnessing them simultaneously should be more efficient and convenient. Notably, elongated TiO_2 prepared by Zheng's group showed good performance for simultaneous photocatalytic phenol oxidation and Cr(VI) reduction under UV light [22]. Zhang *et al.* achieved visible light photocatalytic degradation of phenol and chromium through doping bismuth into TiO_2 [23]. Li *et al.* using hydroxylated Fe_2O_3 realized 70.2% ratio of Cr(VI) reduction and 47.8% ratio of 4-chlorophenol oxidation synergistically under high power Xe lamp

* Corresponding authors.
E-mail addresses: shenxiaoqing@zzu.edu.cn (X. Shen), chenhaijun@zzu.edu.cn (H. Chen).

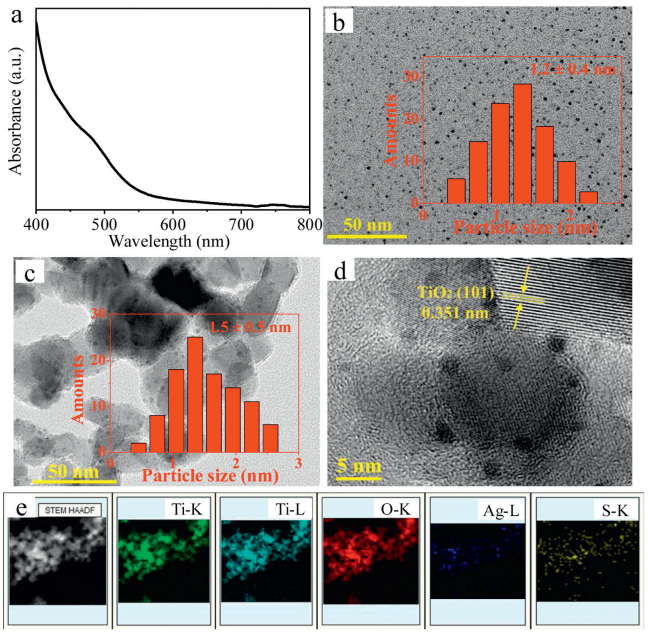

Fig. 1. (a) UV–vis absorption spectra. (b) TEM image and size distribution histogram (insert) of $Ag_m(SR)_n$. (c) TEM image and size distribution histogram (insert) of $Ag_m(SR)_n$/P25. (d) HRTEM image of $Ag_m(SR)_n$/P25. (e) EDX mapping of the $Ag_m(SR)_n$/P25.

[24]. However, most of the above studies either carried out under UV light or could not achieve high degradation efficiency for both organic and inorganic pollutants simultaneously.

Herein, we report a simple and effective strategy to synthesize ultrasmall $Ag_m(SR)_n$ nanoclusters. The $Ag_m(SR)_n$ loaded on P25 shows excellent photodegradation performance on methyl orange (MO) under low power LED lamp (5 W), which is a long life span, high energy efficiency, cost effective, and mercury free lamp compared to mercury lamp or high-energy xenon lamp. Moreover, this $Ag_m(SR)_n$/P25 catalyst also exhibits high photocatalytic activity for the simultaneous degradation of two kinds of pollutants, *i.e.*, one organic (MO, 4-chlorophenol) being oxidized and the other inorganic (Cr(VI)) being reduced.

Thiolate protected $Ag_m(SR)_n$ (SR presents 3-mercaptopropyltriethoxysilane) nanoclusters were prepared by a modified size focusing method (details in Supporting information). Briefly, 3-mercaptopropyltriethoxysilane was added to etch $Ag(PPh_3)_3Cl$ followed by reduction using $NaBH_4$ [25]. The UV–vis absorption spectrum in Fig. 1a showed an absorption peak at 480 nm, which is different from the surface plasmon absorption of Ag nanoparticles (NP) [26–30], indicating the possibility of non-metallic nature of the silver clusters [31]. The morphology and size of $Ag_m(SR)_n$ nanoclusters were analyzed by transmission electron microscopy (TEM). As shown in Fig. 1b, the $Ag_m(SR)_n$ nanoclusters are almost monodisperse with an average size of 1.20 nm, which shows that the particles synthesized are very small and may only consist of a few atoms (less than 100) [32]. Then, $Ag_m(SR)_n$ was supported on P25 by co-hydrolyzing thiolate ligands 3-mercaptopropyltriethoxysilane with the surface hydroxyl of P25 to improve its stability. To acquire comprehensive understanding of the structure of $Ag_m(SR)_n$/P25 catalysts, high-resolution transmission electron microscopy (HRTEM) was used to characterize $Ag_m(SR)_n$/P25. As can be seen from Figs. 1c and d, the silver clusters were uniformly distributed on the surface of P25 with an average size of 1.5 nm (in accordance with that of unsupported clusters). Energy dispersive X-ray (EDX) spectroscopy analysis of the catalysts showed that silver and sulfur species were uniformly distributed on the P25 (Fig. 1e). The results illustrate that being loaded onto P25 can prevent $Ag_m(SR)_n$ nanoclusters with thiolate ligands from aggregating effectively. To further confirm the structure of the silver cluster, the Fourier transform infrared spectrum (FTIR) was conducted for both P25 and $Ag_m(SR)_n$/P25 (Fig. S1 in Supporting information). The stretching vibration peaks of C—H at 2977 cm^{-1} and 2923 cm^{-1} of $Ag_m(SR)_n$/P25 demonstrated that the 3-mercaptopropyltriethoxysilane ligands of $Ag_m(SR)_n$ still existed after being loaded on P25, indicating the intact loading of $Ag_m(SR)_n$.

The optical properties of the as-prepared samples were investigated by UV–vis diffuse reflectance spectroscopy, which was shown in Fig. S2 (Supporting information). The absorption peak of $Ag_m(SR)_n$/P25 gave a red shift to 490 nm, indicating the interaction between silver nanoclusters and P25. For comparison, we prepared Ag nanoparticles (Ag NP) with an average size of 8.0 nm supported on P25 by a photo-reduction method (Fig. S3 in Supporting information). AgNP/P25 had an absorption peak at around 400~600 nm, which is caused by LSPR effect.

To reveal the surface chemical compositions of the photocatalysts, X-ray photoelectron spectroscopy (XPS) analysis was conducted on both AgNP/P25 and $Ag_m(SR)_n$/P25. The full-scan spectra revealed that Ti, O and Ag elements co-exist in the AgNP/P25, while $Ag_m(SR)_n$/P25 composite contained not only Ti, O and Ag elements, but also S (Fig. 2a). These results agree well with the EDX analysis, further confirming the successful loading of silver nanocluster on P25. For an in-depth analysis of the Ag 3d peaks, the corresponding high-resolution XPS spectra of the $Ag_m(SR)_n$/P25 and AgNP/P25 were shown in Figs. 2b and c, respectively. Two distinct peaks centered at 368 eV and 374 eV binding energies correspond to Ag $3d_{5/2}$ and Ag $3d_{3/2}$ of $Ag_m(SR)_n$ respectively, which indicates Ag existed in the form of Ag^+ on the surface of $Ag_m(SR)_n$/P25. The positive charge of Ag arises from the intact thiolate ligands of silver clusters and the existence of thiolates ligands has already been verified by IR results. The S signals of $Ag_m(SR)_n$/P25 XPS spectra (Fig. 2d) further demonstrates the presence of mercapto ligands [33]. The peaks centered at 162.9 eV is in good agreement with the thiolates species, which indicates the formation of S-Ag bond. Another peak at 168.5 eV can be attributed to sulfonates generated due to X-ray beam induced

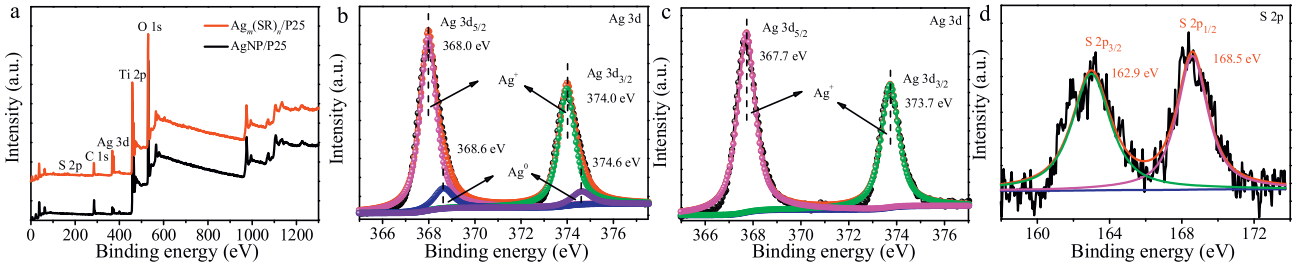

Fig. 2. (a) XPS survey spectra of $Ag_m(SR)_n$/P25 and AgNP/P25. High-resolution XPS spectra of (b) Ag 3d of $Ag_m(SR)_n$/P25, (c) Ag 3d of AgNP/P25, (d) S 2p of $Ag_m(SR)_n$/P25.

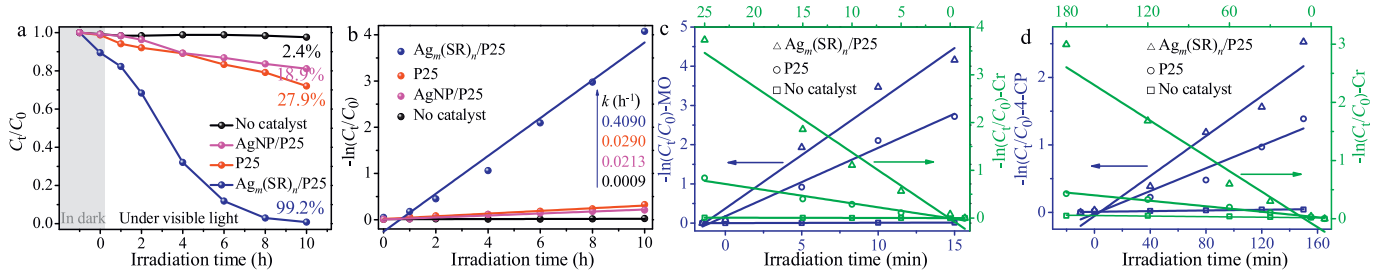

Fig. 3. (a) Photocatalytic degradation efficiencies of MO and (b) *pseudo*-first-order kinetic model with different catalysts under 465 nm blue light. *Pseudo*-first-order kinetic of different catalysts for photocatalytic degradation (465 nm blue-light) of (c) MO and Cr(VI) simultaneously, (d) 4-CP and Cr(VI) simultaneously.

oxidation of thiolates [34]. It should be note that two peaks centered at 368 eV and 374 eV binding energies in Fig. 2b attributed to Ag^0, indicating the core of the silver clusters were not bound to thiolates. This core-shell structure of silver nanocluster may contribute to its photocatalytic activity [3]. To be contrast, the signals of Ag in Fig. 2c manifest the presence of Ag^+ species in AgNP/P25. The formation of positive charge silver is ascribed to the Ag particles binding strongly to P25 surfaces instead of a simple adsorption on P25 surfaces, which has been reported by Huang *et al.* [35] and Cheng *et al.* [36].

The photocatalytic activities of the as-prepared samples were evaluated using methyl orange (MO) as a model contaminant under a 5 W blue LED lamp (460–470 nm). As shown in Fig. 3a, the dark region signified that the system was stirred in the dark for 1 h to assure the establishment of adsorption-desorption equilibrium between the catalysts and reactant. The degradation of MO can be neglected under visible light in the absence of the catalyst. The pure P25 sample exhibited low photocatalytic degradation activity with 27.9% MO decomposed. The photo catalytic efficiency of AgNP/P25 was only about 18.9% under identical conditions, which showed no obvious improved catalytic activity compared with P25, indicating inconspicuous photosensitized degradation. However, the degradation activity of $Ag_m(SR)_n$/P25 significantly improved to 99.2%, indicating the distinct role of silver nanoclusters. It should be note that the stronger adsorption of $Ag_m(SR)_n$/P25 (10.7%) on MO than that of AgNP/P25 (1.2%) was facilitated to the high catalytic activity and all the degradation data was the average of repeating for three times. In addition, the *pseudo*-first-order kinetic model was expressed by Eq. 1 to describe the photocatalytic degradation process of MO, where k is the rate constant of *pseudo*-first-order kinetics and t was the irradiation time. Fig. 3b displayed a nearly straight line for the plots of irradiation time *versus* the $-\ln(C_t/C_0)$, and the k for $Ag_m(SR)_n$/P25 was 0.4090 h^{-1}, which was about 14 times of pure P25 and 19 times of AgNP/P25.

$$\ln(C_t/C_0) = -kt \quad (1)$$

To further test the applicability of $Ag_m(SR)_n$/P25 catalysts, green LED light (505 nm) was applied to conducted the degradation. Fig. S4 (Supporting information) showed that the degradation rate of $Ag_m(SR)_n$/P25 on MO were 5 and 10 times higher than those of P25 and AgNP/P25. Moreover, simultaneous photocatalytic MO oxidation and Cr(VI) reduction, 4-chlorophenol oxidation and Cr(VI) reduction, were conducted since the inorganic and organic pollutions usually co-exist in waste water. The degradation rate of MO was increased steeply to 0.273 min^{-1} (*vs.* 0.409 h^{-1}, Figs. 3b and c) when Cr(VI) existed in the system, in which situation both electrons and hole can be consumed, and the consumption of electrons by Cr(VI) reduction further promoted photo-generated carriers separated efficiency of $Ag_m(SR)_n$/P25. It should be pointed that MO oxidation and Cr(VI) reduction rates catalyzed by $Ag_m(SR)_n$/P25 were 1.6 and 4.4 times higher than that of P25, respectively (Fig. 3c). Similar situation also occurred for 4-chlorophenol oxidation and Cr(VI) reduction, where 4-chlorophenol oxidation and Cr(VI) reduction rates catalyzed by $Ag_m(SR)_n$/P25 were 1.8 and 7.5 times higher than that of P25, respectively (Fig. 3d). No pollutants were diminished without catalysts for all the systems under LED irradiation.

In order to investigate the influence of structural variation of silver nanocluster on the catalytic activity of $Ag_m(SR)_n$/P25, the catalysts was treated at different temperature. After the calcination, the size of the silver nanocluster gradually grew up (Figs. S5a-c in Supporting information). The XPS spectrum of S signals of $Ag_m(SR)_n$/P25 calcined at 500 °C (Fig. S5d in Supporting information) demonstrates that almost no thiolate ligands existed after the calcination. The ligands are very vital to the metal nanoclusters to sustain their structures and the corresponding chemical nature [37,38]. The removal of SR ligands would result in Ag cores exposed and then agglomerated to larger ones. Fig. S6a (Supporting information) showed that the photocatalytic activity of the calcined $Ag_m(SR)_n$/P25 was gradually decreased. Thus, sustaining the intact structure of $Ag_m(SR)_n$ with thiolate ligands is essential to the catalytic activity of the catalysts.

To further investigate the photocatalytic degradation mechanism of $Ag_m(SR)_n$/P25 and reveal the contribution of the primarily active radical species during the degradation reaction, different charge scavengers were introduced into the degradation of MO [39,40]. Ignorable inhibition to the degradation was shown by isopropanol (IPA), indicating that the $^{\bullet}OH$ almost does not contribute to the degradation of MO (Fig. 4a). This is different from the degradation mechanism of P25 on organic compounds, in the system of which $^{\bullet}OH$ is usually the main active species [41], indicating the decisive role of $Ag_m(SR)_n$ nanoclusters. The degradation efficiency of MO was significantly inhibited to only 34.7% using ammonium oxalate (AO) as a scavenger compared with 99.2%, indicating the indispensable role of holes generated by Ag nanoclusters. Moreover, the degradation efficiency of MO was significantly increased to 96.8% by adding $K_2S_2O_8$, which is an electron scavenger. It is noteworthy that $K_2S_2O_8$ itself can only degrade 9.1% of MO under visible, while adding $K_2S_2O_8$ into $Ag_m(SR)_n$/P25 can degrade 28.5% of MO under dark conditions (Fig. 4b), indicating that $K_2S_2O_8$ had almost no degradation activity on MO. Therefore, there is a synergistic effect between $Ag_m(SR)_n$/P25 and $K_2S_2O_8$ under visible light. The main reason is that the addition of $K_2S_2O_8$ can capture e^-, thus inhibiting the recombination of electron hole pairs and increasing the availability of h^+ species in the reaction system [42].

The *p*-benzoquinone (BQ) significantly inhibited the degradation efficiency to 10% (Fig. 4a), indicating that the $O_2^{\bullet-}$ is involved in the catalytic degradation process [43,44]. Further, Fig. 4c exhibited that when the $Ag_m(SR)_n$/P25 was exposed to visible light, six typical $O_2^{\bullet-}$ signals were detected by electron spin resonance (ESR), while in the dark there was no signal, demonstrating that $O_2^{\bullet-}$ is formed in the process. However, pure P25 did not track significant signals in both dark and light conditions. These results clearly

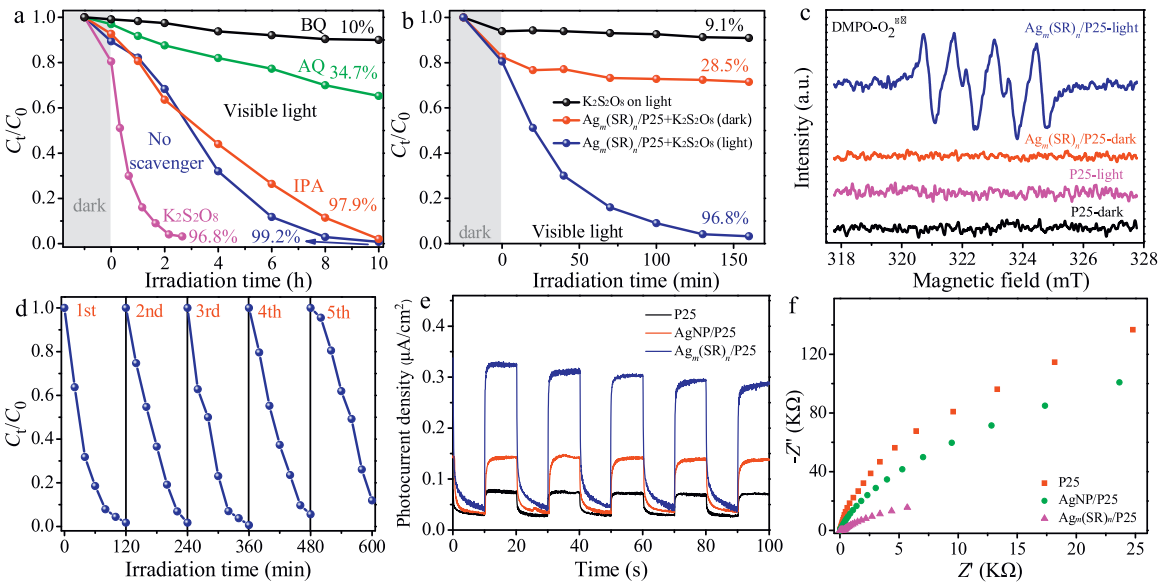

Fig. 4. (a) Photocatalytic degradation of MO with different scavengers under 465 nm blue light. (b) Photocatalytic degradation of MO by $Ag_m(SR)_n$/P25 and $K_2S_2O_8$ under 465 nm blue light. (c) ESR spectra (white light), (d) cycling runs (465 nm blue-light), (e) photocurrent responses (white light) and (f) EIS of the P25, AgNP/P25 and $Ag_m(SR)_n$/P25.

demonstrated that $O_2^{\bullet-}$ is also the main active specie in the photocatalytic degradation process of $Ag_m(SR)_n$/P25. Fig. 4d showed that after five consecutive cycles in the presence of $K_2S_2O_8$, the photocatalytic activity of $Ag_m(SR)_n$/P25 on MO degradation can also be maintained at a high level, indicating the good photo-stability of the as-prepared samples.

To reveal the origin of the higher catalytic activity of $Ag_m(SR)_n$/P25, photocurrent response, electrochemical impedance spectroscopy (EIS) and photoluminescence were used to evaluate the separation efficiency of the photogenerated electron and hole pairs. As shown in Fig. 4e, the photocurrent density of $Ag_m(SR)_n$/P25 was significantly higher than those of AgNP/P25 and pure P25, exhibiting an enhanced photocurrent density. The arc radius of the EIS Nyquist plot of the $Ag_m(SR)_n$/P25 was the smallest among all of the catalysts (Fig. 4f), verifying that the $Ag_m(SR)_n$/P25 had the lowest electron transfer resistance. The photoluminescence spectroscopy in Fig. S7 (Supporting information) showed that $Ag_m(SR)_n$/P25 gave a lower fluorescence intensity, implying the lower electron and hole recombination efficient of $Ag_m(SR)_n$/P25. All the above results indicated that $Ag_m(SR)_n$/P25 exhibited an enhanced separation efficiency of charge carrier, which could be attributed to the core-shell structure and quantum confinement effects of $Ag_m(SR)_n$ with discrete electronic structure.

According to the experimental results and analyses, the probable mechanism thus is proposed and shown in Fig. 5. The role of $Ag_m(SR)_n$ nanoclusters is similar to that of narrow band gap semiconductors, and its LUMO energy level is equivalent to the flat band potential of semiconductors, which can be measured by Mott-Schottky plots [45]. The photo-generated electrons of $Ag_m(SR)_n$ are injected into P25 because the LUMO energy level of $Ag_m(SR)_n$ (−0.58 V *vs.* Ag/AgCl) is higher than the conduction potential (−0.26 V *vs.* Ag/AgCl) of P25 determined by the Mott-Schottky plots (Fig. S8 in Supporting information). The excited electrons can reduce the O_2 to $O_2^{\bullet-}$species and also reduce Cr(VI) to Cr(III) in the simultaneous degradation both organic and inorganic pollutants system. The MO and 4-chlorophenol are oxidized by $O_2^{\bullet-}$ in addition to holes.

In summary, we developed an effective method to synthesize ultrasmall $Ag_m(SR)_n$, which exhibited outstanding photocatalytic activity for the photocatalytic degradation of MO under both blue and green light. Moreover, simultaneous oxidation of MO/4-chlorophenol and reduction of Cr(VI) are smoothly achieved by $Ag_m(SR)_n$/P25. The ultra-high photocatalytic activity of the nanocluster was mainly attributed to the core-shell structure, quantum size effect and high photo-generated carriers' separation efficiency of silver nanoclusters. The $Ag_m(SR)_n$/P25 also exhibited excellent recycling stability. This work demonstrates the great potential of nanoclusters for visible light-driven environmental remediation ability with high performance.

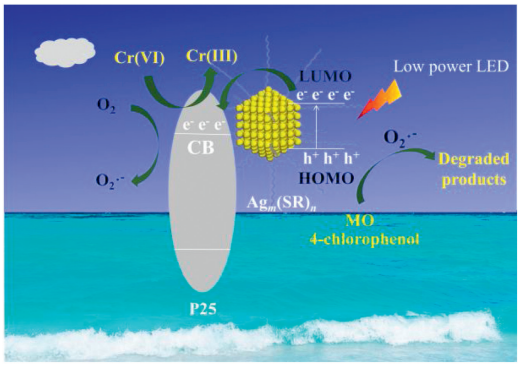

Fig. 5. The proposed mechanism for photocatalytic degradation catalyzed by $Ag_m(SR)_n$/P25.

Declaration of competing interest

The authors declare that they have no known competing financial interests or personal relationships that could have appeared to influence the work reported in this paper.

Acknowledgment

This work was supported by the National Natural Science Foundation of China (No. 21671176).

Appendix A. Supplementary data

Supplementary material related to this article can be found, in the online version, at doi:https://doi.org/10.1016/j.cclet.2020.06.002.

References

[1] B. Han, E. Wang, Anal. Bioanal. Chem. 402 (2012) 129–138.
[2] S. Choi, R.M. Dickson, J. Yu, Chem. Soc. Rev. 41 (2012) 1867–1891.
[3] H. Qian, M. Zhu, Z. Wu, R. Jin, Acc. Chem. Res. 45 (2012) 1470–1479.
[4] Y. Lu, W. Chen, Chem. Soc. Rev. 41 (2012) 3594–3623.
[5] H. Xu, K.S. Suslick, Adv. Mater. 22 (2010) 1078–1082.
[6] X. Nie, H. Qian, Q. Ge, H. Xu, R. Jin, ACS Nano 6 (2012) 6014–6022.
[7] J. Liu, H. Wang, M. Antonietti, Chem. Soc. Rev. 45 (2016) 2308–2326.
[8] J. Cai, J. Huang, S. Wang, et al., Adv. Mater. 31 (2019) e1806314.
[9] S. Malato, P. Fernandez-Ibanez, M.I. Maldonado, J. Blanco, W. Gernjak, Catal. Today 147 (2009) 1–59.
[10] U.I. Gaya, A.H. Abdullah, J. Photochem. Photobiol. C 9 (2008) 1–12.
[11] N. Serpone, A.V. Emeline, J. Phys. Chem. Lett. 3 (2012) 673–677.
[12] S. Ghosh, N.A. Kouame, L. Ramos, et al., Nat. Mater. 14 (2015) 505–511.
[13] M. Pelaez, N.T. Nolan, S.C. Pillai, et al., Appl. Catal. B: Environ. 125 (2012) 331–349.
[14] L. Suljo, C. Phillip, D.B. Ingram, Nat. Mater. 10 (2011) 911–921.
[15] J. Zhang, X. Jin, P.I. Morales-Guzman, et al., ACS Nano 10 (2016) 4496–4503.
[16] S. Xu, L. Guo, Q. Sun, Z. Wang, Adv. Funct. Mater. 29 (2019) 1–8.
[17] Z. Chen, L. Fang, W. Dong, et al., J. Mater. Chem. A 2 (2014) 824–832.
[18] J. Zhao, S.C. Nguyen, R. Ye, et al., ACS Cent. Sci. 3 (2017) 482–488.
[19] M.A. Abbas, P.V. Kamat, J.H. Bang, ACS Energy Lett. 3 (2018) 840–854.
[20] F. Xiao, S. Hung, J. Miao, et al., Small 11 (2015) 554–567.
[21] G. Zhang, R. Wang, G. Li, Chin. Chem. Lett. 29 (2018) 687–693.
[22] R. Mu, Z. Xu, L. Li, et al., J. Hazard. Mater. 176 (2010) 495–502.
[23] S. Sajjad, S.A. Leghari, F. Chen, J. Zhang, Chemistry 16 (2010) 13795–13804.
[24] J. Wang, J. Ren, H. Yao, et al., J. Hazard. Mater. 311 (2016) 11–19.
[25] A. Cassel, Acta Crystallogr. Sect. B 37 (1981) 229–231.
[26] W. Gao, M. Wang, C. Ran, et al., Nanoscale 6 (2014) 5498–5508.
[27] J. He, I. Ichinose, T. Kunitake, A. Nakao, Langmuir 18 (2002) 10005–10010.
[28] T. Wang, P. Raghunath, Y. Lin, M. Lin, J. Phys. Chem. C 121 (2017) 9681–9690.
[29] Y. Lu, Q. Shen, Q. Yu, et al., J. Phys. Chem. C 120 (2016) 28712–28716.
[30] E. Pulido Melián, O. González Díaz, J. Doña Rodríguez, et al., Appl. Catal. B: Environ. 127 (2012) 112–120.
[31] W. Chen, Y. Hsu, P. Kamat, J. Phys. Chem. Lett. 3 (2012) 2493–2499.
[32] J. Wilcoxon, B. Abrams, Chem. Soc. Rev. 35 (2006) 1162–1194.
[33] H. Chen, Z. Li, Z. Qin, et al., ACS Appl. Nano Mater. 2 (2019) 2999–3006.
[34] S. Pethkar, M. Aslam, I. Mulla, P. Ganeshan, K. Vijayamohanan, J. Mater. Chem. 11 (2001) 1710–1714.
[35] H. Zheng, Z. Jiang, H. Zhai, et al., Appl. Catal. B: Environ. 243 (2019) 381–385.
[36] X. Wang, Z. Zhao, D. Ou, et al., Appl. Surf. Sci. 385 (2016) 445–452.
[37] T. Higaki, Y. Li, S. Zhao, et al., Angew. Chem. Int. Ed. 58 (2019) 8291–8302.
[38] Y. Wang, X.K. Wan, L. Ren, et al., J. Am. Chem. Soc. 138 (2016) 3278–3281.
[39] Y. Duan, J. Luo, S. Zhou, et al., Appl. Catal. B: Environ. 234 (2018) 206–212.
[40] C. Zhang, Z. Huang, J. Lu, N. Luo, F. Wang, J. Am. Chem. Soc. 140 (2018) 2032–2035.
[41] C. Turchi, D. Ollis, J. Catal. 122 (1990) 178–192.
[42] A. Rupa, D. Manikandan, D. Divakar, T. Sivakumar, J. Hazard. Mater. 147 (2007) 906–913.
[43] Y. Li, J. Wang, H. Yao, L. Dang, Z. Li, J. Mol. Catal. A: Chem. 334 (2011) 116–122.
[44] W. Li, Y. Tian, H. Li, et al., Appl. Catal. A: Gen. 516 (2016) 81–89.
[45] C. Ren, W. Li, H. Li, et al., Appl. Surf. Sci. 408 (2019) 96–104.